Hindrance Factors for Diffusion and Convection in Pores

Panadda Dechadilok[†] and William M. Deen*[,‡]

Division of Engineering and Applied Sciences, Harvard University, Cambridge, Massachusetts 02138, and Department of Chemical Engineering, Massachusetts Institute of Technology, Cambridge, Massachusetts 02139

It is well-known that solutes in liquid-filled pores of molecular dimensions have reduced diffusivities and are sieved during filtration. For solute molecules that are large enough to act as hydrodynamic particles, these phenomena can be explained by a combination of particle−wall hydrodynamic interactions and steric restrictions. Theoretical expressions that include those effects have been available for many years, but, even for spheres in pores of constant cross-section, certain hydrodynamic information has been lacking until recently. In particular, the local enhanced drag and local lag coefficient for off-axis positions had not been fully characterized, requiring that results for symmetrically positioned particles ("centerline approximations") be employed in predicting diffusional and convective hindrances. In this paper the current status of hindered transport theory is reviewed for neutral spheres in long cylindrical pores or slits, and it is shown that such approximations are no longer necessary. New expressions are presented for diffusive and convective hindrance factors that are properly averaged over the pore cross-section. The root-mean-square errors in the centerline approximations are 19% and 6%, respectively, for diffusive and convective hindrance factors in cylindrical pores; for slit pores the corresponding errors are 25% and 10%. Comparisons are made between the predictions and recent data obtained by tracking particle positions in microchannels.

Introduction

A solute molecule that is at least several times larger than a solvent molecule can be viewed as a Brownian particle that experiences a hydrodynamic resistance to its motion. As derived by Einstein in 1905, the diffusivity of such a molecule in an unbounded liquid equals the thermal fluctuation energy divided by the drag coefficient.[1] For a spherical solute, the result is the Stokes−Einstein equation. In pores of molecular dimensions, the diffusivity of the solute is reduced and the solute is sieved during filtration. These hindrances to diffusion and convection are attributable to a combination of particle−wall hydrodynamic interactions and steric restrictions. The hydrodynamic interactions depend on how close the particle is to the wall, and they are therefore affected by any force that influences its position. Even if long-range (e.g., van der Waals or electrostatic) forces are negligible, the finite size of the solute restricts its access to the region near the wall and therefore affects its flux.

As reviewed in Deen,[2] the pioneering developments in hindered transport theory in the early 1950s were motivated by a desire to understand the effects of molecular size on microvascular permeability. Other applications to biological and synthetic membranes followed, as did experimental tests using track−etch membranes with uniform pores of known size. Theories aimed at predicting hindered transport coefficients from the size, shape, and electrical charge of solutes and pores had undergone several refinements by the time of that review. A continuing interest in hindered transport theory is evidenced by more recent studies of drug delivery through skin,[3] protein diffusion in cellular microtubules,[4] the selectivity of asymmetric ultrafiltration membranes,[5] and on-chip hydrodynamic chromatography,[6] to cite a few examples. Because the aforementioned review is nearly 20 years old, and because subsequent results permit improved predictions of diffusive and convective hindrance factors, an update of the theory is timely.

In this paper we focus on the most basic situation, involving uncharged, spherical particles in long pores of uniform cross-section. Results will be presented for both cylindrical and slit pores (parallel-plate channels). First, the diffusive and convective hindrance factors that appear in either local or macroscopic flux expressions will be defined. Then, available numerical and analytical results for the required hydrodynamic coefficients will be discussed and new correlations for the hindrance factors presented. Finally, comparisons will be made between the updated theory and recent experimental data.

Hindrance Factor Definitions for Local Fluxes

As already indicated, the linear dimensions of the solute molecule are assumed here to be much greater than those of the solvent. Accordingly, the solute is treated as a particle and the solvent as a continuum. The small length and velocity scales ensure Reynolds numbers small enough to make Stokes' equation applicable. The pore length is assumed to be much larger than its diameter or width, which has three main consequences. First, the solute particles will have time to sample all cross-sectional positions many times during passage through a pore. If there is an imposed bulk flow, this requires also that the Peclet number based on the pore radius or half-width be small.[7] Second, the flow (if any) will be fully developed, and end effects on the velocity profile will be negligible. Third, the mass transfer resistances at the pore ends will be negligible, allowing internal and external solute concentrations to be related by an equilibrium partition coefficient. For membrane applications, Taylor dispersion is negligible.[2] The version of the theory discussed here is restricted to dilute solutions and to situations where long-range forces are negligible. Thus, solute−solute interactions are absent and all coefficients are concentration-independent. See Deen[2] for a discussion of charge and concentration effects.

[†] Harvard University.

[‡] Massachusetts Institute of Technology.

* To whom correspondence should be addressed. Address: Department of Chemical Engineering, 66-572, Massachusetts Institute of Technology, 77 Massachusetts Avenue, Cambridge, MA 02139. Tel.: (617) 253-4535. Fax: (617) 253-2072. E-mail: wmdeen@mit.edu.

10.1021/ie051387n CCC: $33.50
Published on Web 03/09/2006 **PAGE EST: 6.5**

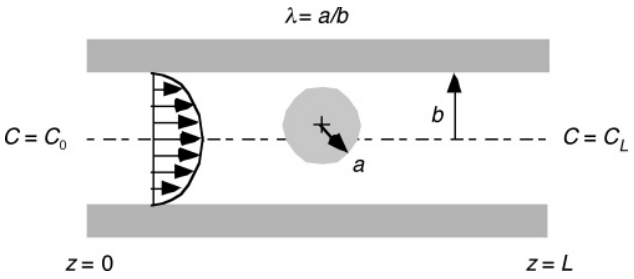

Figure 1. Spherical solute of radius a in a pore of molecular dimensions. For a cylindrical pore, b is the radius; for a slit, b is the half-width. The relative solute size is $\lambda = a/b$.

The coordinates and geometric quantities are defined in Figure 1. The solute radius is a, and the pore radius or half-width is b. The key parameter is the relative solute size, $\lambda = a/b$. The pore extends from $z = 0$ to $z = L$, and the dimensionless coordinate normal to its axis (scaled by b) is denoted as β. For cylindrical pores, $0 \le \beta \le 1$; for slit pores, $-1 \le \beta \le 1$, but only non-negative values need be considered because of the symmetry.

With these assumptions, the axial component of the solute flux can be written as

$$\langle N\rangle = -K_d D_\infty \frac{d\langle C\rangle}{dz} + K_c\langle V\rangle\langle C\rangle \qquad (1)$$

where N is the flux, C is the concentration, V is the unperturbed (parabolic) fluid velocity, and the angle brackets indicate averages over the pore cross-section. The diffusivity in an unbounded solution is D_∞, and K_d and K_c are local hindrance factors for diffusion and convection, respectively. For either pore shape, K_d declines monotonically as λ increases; diffusion is not hindered in large pores ($K_d \to 1$ for $\lambda \to 0$), but vanishes for tightly fitting solutes ($K_d \to 0$ for $\lambda \to 1$). The behavior of K_c is more complicated. Although $K_c \to 1$ for $\lambda \to 0$, whether K_c vanishes for $\lambda \to 1$ depends on the pore shape, as will be explained later. Also, $K_c(\lambda)$ is not monotonic, but first increases with λ and then decreases. For intermediate λ, where $K_c > 1$, the dominant effect is steric exclusion from the wall region, which prevents the particles from sampling the most slowly moving fluid. (The size-dependent increase in K_c is the basis for hydrodynamic chromatography.)

For spheres in *cylindrical pores*, the hindrance factors are related to the relevant hydrodynamic coefficients by

$$K_d(\lambda) = \frac{2}{(1-\lambda)^2}\int_0^{1-\lambda} \frac{\beta\, d\beta}{K(\lambda,\beta)} \qquad (2)$$

$$K_c(\lambda) = \frac{4}{(1-\lambda)^2}\int_0^{1-\lambda} G(\lambda,\beta)(1-\beta^2)\beta\, d\beta \qquad (3)$$

where K is the *enhanced drag* (drag coefficient relative to that in an unbounded fluid) and G is the *lag coefficient* (velocity of the particle relative to the unperturbed velocity evaluated at the particle center). For spheres in *slit pores*, the analogous expressions are

$$K_d(\lambda) = \frac{1}{(1-\lambda)}\int_0^{1-\lambda} \frac{d\beta}{K(\lambda,\beta)} \qquad (4)$$

$$K_c(\lambda) = \frac{3}{2(1-\lambda)^2}\int_0^{1-\lambda} G(\lambda,\beta)(1-\beta^2)\, d\beta \qquad (5)$$

Details of the averaging that leads to eqs 1−5 can be found in Deen.[2]

In either geometry, the evaluation of the enhanced drag and lag coefficient is facilitated by the existence of a symmetric 3 × 3 matrix that relates the drag, torque, and excess pressure drop to the translational velocity of the sphere, the angular velocity of the sphere, and the mean fluid velocity.[8] The enhanced drag can be obtained by calculating the force and torque on a sphere in two situations with no mean flow: (i) a nonrotating sphere translating parallel to the pore axis at a given velocity and (ii) a stationary sphere rotating at a given angular velocity. Such results yield the coefficients that relate the force and torque to the translational and angular velocities, and thereby allow calculation of the drag on a freely rotating (torque-free) sphere, as desired. The lag coefficient can be obtained by computing the force, torque, and excess pressure drop for (i), (ii), and an additional case: (iii) Poiseuille flow at a given mean velocity past a stationary sphere. What is sought in this case is the velocity of a freely suspended (force- and torque-free) sphere relative to the unperturbed Poiseuille flow. Of importance, K and G are local quantities that depend on the position of the particle center (β), as well as particle size (λ). For symmetrically positioned spheres ($\beta = 0$), the torque and angular velocity are each identically zero and the calculations are simplified; the drag coefficient is obtained directly from the force for case (i), and the lag coefficient equals the force for case (iii) divided by that for case (i). Also, for $\beta = 0$ in cylindrical channels, the problem is two-dimensional (axisymmetric) rather than three-dimensional.

Hindrance Factor Definitions for Overall Fluxes

In membrane processes or other applications where it is desired to relate a steady or pseudo-steady flux to the external concentrations, a macroscopic flux expression is more useful than the local one given by eq 1. Assuming constancy of $\langle N\rangle$, as in a steady state without chemical reactions, integration of eq 1 gives

$$\langle N\rangle = \Phi K_c\langle V\rangle C_0 \frac{[1-(C_L/C_0)\, e^{-Pe}]}{1-e^{-Pe}} \qquad (6)$$

where C_0 and C_L are the external solute concentrations at $z = 0$ and $z = L$, respectively, and Φ is the equilibrium partition coefficient. The partition coefficient is the cross-sectional average concentration at either pore end divided by the adjacent external concentration. The membrane Peclet number that appears in eq 6 is

$$Pe = \frac{\Phi K_c\langle V\rangle L}{\Phi K_d D_\infty} \qquad (7)$$

The common factor Φ in the numerator and denominator has been retained for reasons given below. When the downstream concentration is determined entirely by the transmembrane fluxes (as is often the case in ultrafiltration), $C_L = \langle N\rangle/\langle V\rangle$ and eq 6 is replaced by

$$\langle N\rangle = \frac{\Phi K_c\langle V\rangle C_0}{1-(1-\Phi K_c)\, e^{-Pe}} \qquad (8)$$

Inspection of eqs 6−8 reveals that transmembrane fluxes written in terms of external concentrations depend only on the products, ΦK_d and ΦK_c, and not the three individual quantities involved. Accordingly, we define

$$H(\lambda) = \Phi(\lambda)\, K_d(\lambda) \quad (9)$$

$$W(\lambda) = \Phi(\lambda)\, K_c(\lambda) \quad (10)$$

where H and W are overall hindrance factors for diffusion and convection, respectively. For purely steric interactions between a sphere and a *cylindrical pore*, the equilibrium partition coefficient is given by[2,9]

$$\Phi(\lambda) = (1 - \lambda)^2 \quad (11)$$

For a sphere in a *slit pore*, the analogous expression is

$$\Phi(\lambda) = (1 - \lambda) \quad (12)$$

In either case, Φ is equivalent to the fraction of the cross-sectional area of the pore that is accessible to the sphere center. Results for H or W are obtained by multiplying the expressions for K_d or K_c given earlier by the appropriate expression for Φ.

In summary, K_d and K_c are the hindrance factors needed to calculate fluxes from local intrapore concentrations, and H and W are the ones needed for use with external concentrations. Most of the results to be presented are for H and W, but they are readily converted to K_d and K_c using eqs 9−12, if desired.

Hydrodynamic Results and Hindrance Factor Correlations

Equations 2−5 have been known for many years, and the limiting factor in calculating the hindrance factors has been obtaining values of K and G for sufficient ranges of λ and β. Results for symmetrically positioned spheres have been more available than ones for off-axis positions, so that it has been common to employ *centerline approximations* in which the local enhanced drag and local lag coefficient are replaced by $K(\lambda, 0)$ and $G(\lambda, 0)$, respectively.[2] In this section, numerical and analytical results for the hindrance factors are presented for cylindrical pores and then slit pores. For each pore shape, we begin with a brief review of centerline approximations and then move to more recent work that employs off-axis results. Correlations are provided that represent the properly averaged hindrance factors, first for diffusion and then for convection.

Cylindrical Pores. A. Centerline Approximations. The pioneering estimates of $H(\lambda)$, involving a centerline approximation and contributions to K_d up to order λ, were those of Pappenheimer et al.[10] Using centerline drag coefficients from Lane,[11] Renkin[12] obtained

$$H(\lambda) = (1 - \lambda)^2(1 - 2.104\lambda + 2.09\lambda^3 - 0.95\lambda^5) \quad (13)$$

This much-quoted result, called the *Renkin equation*, is restricted to $\lambda \leq 0.4$.

Haberman and Sayre,[13] Wang and Skalak,[14] and Paine and Scherr[15] all provided numerical results in tabular form that improved centerline estimates of K and G. Bean,[16] who was the first to recognize the need for the lag coefficient, calculated K and G up to terms involving λ^{10}. Bungay and Brenner,[8] using asymptotic matching, obtained results for K and G that were reported to have better than 1% accuracy for $0 \leq \lambda \leq 1$. Their expressions, which involve a total of 14 coefficients, are summarized also in Deen[2]. Several subsequent studies have confirmed the accuracy of their results. Bowen and Sharif[17] calculated both K and G using finite elements. Their results led to expressions provided by Bowen et al.,[18] which are simpler than those of Bungay and Brenner[8] but valid only for $\lambda \leq 0.8$. Feng and Michaelides[19] calculated K using the Lattice−Boltzmann method, and Ben Rishou et al.[20] used conformal mapping and finite differences to obtain K and G. Their results are graphically indistinguishable from those of Bungay and Brenner.[8]

B. Cross-Sectional Averaging for Diffusion. The first results that included the radial dependence of the enhanced drag were valid only for limited ranges of particle size. Brenner and Gaydos,[7] employing singular perturbation and asymptotic matching, derived an analytical expression for H for $\lambda \to 0$ that included terms up to $o(\lambda)$. Nitsche and Balgi[21] extended that result up to $o(\lambda^2)$, obtaining

$$H(\lambda) = 1 + \frac{9}{8}\lambda \ln \lambda - 1.539\lambda + 1.2\lambda^2 + o(\lambda^2) \quad (14)$$

Mavrovouniotis and Brenner[22] used asymptotic matching to evaluate K_d for $\lambda \to 1$. In terms of H, their result is

$$H(\lambda) = (1 - \lambda)^2\left\{0.984\left(\frac{1 - \lambda}{\lambda}\right)^{5/2} + O\left[\left(\frac{1 - \lambda}{\lambda}\right)^3\right]\right\} \quad (15)$$

Off-axis hydrodynamic results for a wide range of solute sizes were provided finally by Higdon and Muldowney,[23] who used a boundary element method to evaluate $K(\lambda, \beta)$ for $\lambda = 0.05$, 0.1, 0.2, ..., 0.9. For each value of λ, the results for K were expressed as continuous functions of β. From those results, we evaluated the integral in eq 2 to obtain K_d and H for $0 \leq \lambda \leq 0.9$. Those data were supplemented by using eq 15 to evaluate $H(0.95)$. A least-squares fit to the full set of H values for $0 \leq \lambda \leq 0.95$ (minimizing relative errors) yielded

$$H(\lambda) = 1 + \frac{9}{8}\lambda \ln \lambda - 1.56034\lambda + 0.528155\lambda^2 + 1.91521\lambda^3 - 2.81903\lambda^4 + 0.270788\lambda^5 + 1.10115\lambda^6 - 0.435933\lambda^7 \quad (16)$$

Whereas the logarithmic term was retained as is from eq 14, the coefficients of λ and λ^2 were modified to optimize the overall fit. Equation 16 represents the results from Higdon and Muldowney[23] for $0 \leq \lambda \leq 0.9$, and that of Mavrovouniotis and Brenner[22] for $\lambda = 0.95$, to within 0.6%. If it is desired to achieve high precision for more closely fitting spheres ($\lambda > 0.95$), then eq 15 should be used instead.

Various results for H in cylindrical pores are compared in Figure 2. Included are the centerline approximation derived from Bungay and Brenner,[8] the asymptotic result for $\lambda \to 0$ (eq 14), the radial averages calculated from the results of Higdon and Muldowney,[23] and our curve fit to the radial averages (eq 16). (Not shown is the Renkin equation, which is indistinguishable from the later centerline approximations for $\lambda \leq 0.4$, or the asymptotic result for $\lambda \to 1$ given by eq 15, which does not show up well on this scale.) The overall pattern, of course, is that H declines from 1 to 0 as the relative solute size increases. As can be seen, the curve fit in eq 16 is in excellent agreement with the Higdon and Muldowney results, which we view as exact, and (for small particles) eq 14. The centerline approximation turns out to be remarkably accurate, slightly overestimating H for $\lambda \leq 0.4$ and underestimating it for larger particles, while giving a root-mean-square (rms) error of 19% for $\lambda \leq 0.95$.

Insight into the surprising accuracy of the centerline approximation is provided by Figure 3, which shows the radial dependence of K at selected values of λ, as calculated by Higdon and Muldowney.[23] In each case the relative mobility of a sphere (i.e., K^{-1}) first increases slightly as β increases, and then it declines sharply as the wall is approached. The initial increase nearly compensates for the eventual drop, causing the radial

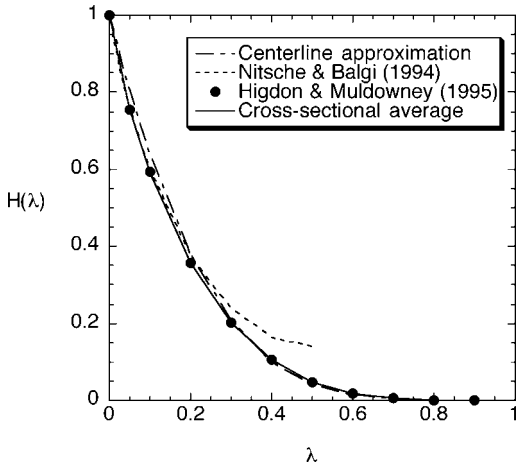

Figure 2. Diffusional hindrance factor (H) for a sphere in a cylindrical pore, as a function of relative particle size (λ). Results based on centerline hydrodynamics[8] are compared with those obtained by radial averaging. The latter include an asymptotic expression from Nitsche and Balgi[21] for $\lambda \rightarrow 0$ (eq 14), numerical results calculated from K of Higdon and Muldowney,[23] and a curve fit to the numerical, cross-sectional averages (eq 16).

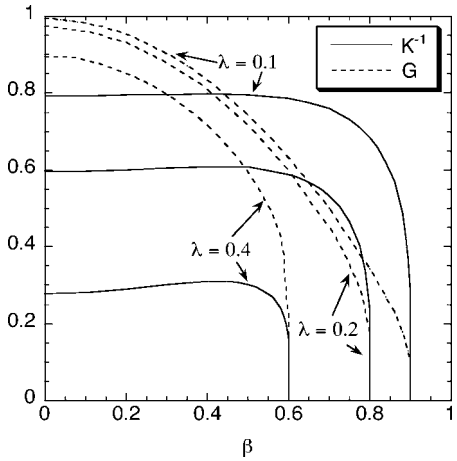

Figure 3. Inverse enhanced drag (K^{-1}) and lag coefficient (G) obtained by Higdon and Muldowney[23] for a sphere in a cylindrical pore, as a function of the position of the sphere center ($\beta = 0$ on the axis and $\beta = 1$ at the wall). Results are given for three relative solute sizes (λ).

average to be close to the centerline value. For slits, where K^{-1} declines monotonically with increasing β,[24] the errors in the centerline approximation are greater, as will be shown.

C. Cross-Sectional Averaging for Convection. Brenner and Gaydos[7] provided asymptotic results for $\lambda \rightarrow 0$ that correspond to

$$W(\lambda) = (1 - \lambda)^2[1 + 2\lambda - 4.9\lambda^2 + o(\lambda^2)] \qquad (17)$$

Higdon and Muldowney[23] evaluated the local lag coefficient, $G(\lambda, \beta)$, for a wide range of λ, allowing us to compute K_c from eq 3 by numerical integration. Ennis et al.[25] used Pade approximation to combine the asymptotic expression for small particles of Brenner and Gaydos[7] with the lubrication results for closely fitting spheres of Bungay and Brenner.[8] In terms of W, their result is

$$W(\lambda) = (1 - \lambda)^2\left(\frac{1 + 3.867\lambda - 1.907\lambda^2 - 0.834\lambda^3}{1 + 1.867\lambda - 0.741\lambda^2}\right) \qquad (18)$$

The results for W in cylindrical pores are compared in Figure 4. Again, the overall hindrance factor declines monotonically

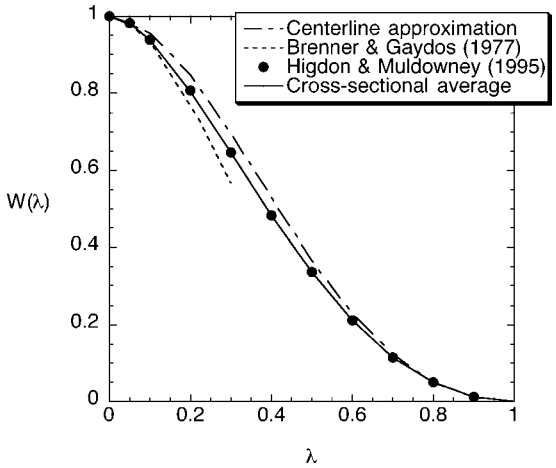

Figure 4. Convective hindrance factor (W) for a sphere in a cylindrical pore, as a function of relative particle size (λ). Results based on centerline hydrodynamics[8] are compared with those obtained by radial averaging. The latter include an asymptotic expression from Brenner and Gaydos[7] for $\lambda \rightarrow 0$ (eq 17), numerical results calculated from G of Higdon and Muldowney,[23] and an expression due to Ennis et al.[24] (eq 18) that closely represents the cross-sectional averages.

as λ is increased. A comparison with Figure 2 indicates that hindrances are less pronounced for convection than for diffusion, such that $W/H > 1$ for intermediate λ. As seen in Figure 4, the Ennis et al. expression (eq 18) converges to the asymptotic result for small particles, and for all particle sizes is graphically indistinguishable from the "exact" results derived from Higdon and Muldowney.[23] Thus, eq 18 provides an excellent representation of the radially averaged convective hindrance factor for all particle sizes. Also shown is that the centerline approximation (again based on Bungay and Brenner[8]) consistently overestimates W, although with a rms error of only 6%. It is worth noting that although the percentage errors for W tend to be smaller than those for H, the absolute errors are larger. Thus, on the linear scales in Figures 2 and 4, the centerline approximation for convection looks less accurate than that for diffusion.

Included in Figure 3 is the radial dependence of G at selected values of λ, as calculated by Higdon and Muldowney.[23] As shown, G decreases monotonically as β increases. A similar trend is observed for a particle confined in a slit pore.[24] It follows that the centerline approximation overestimates $W(\lambda)$ for all values of λ, both in cylindrical pores and (as will be shown) in slits.

Dividing the right-hand side of eq 18 by $(1 - \lambda)^2$ yields K_c for a cylindrical pore. It is found that $K_c \rightarrow 1$ for $\lambda \rightarrow 0$, that it reaches a maximum of about 1.35 at $\lambda \cong 0.5$, and that it decreases again to 1 as $\lambda \rightarrow 1$. The reason that K_c in a cylindrical pore does not vanish for $\lambda \rightarrow 1$ is that a closely fitting sphere acts as a piston, and therefore moves at the mean fluid velocity.

Slit Pores. A. Centerline Approximations. As with cylindrical pores, centerline results for spheres in slits preceded those for off-axis positions. Using the method of reflections, Faxen (as given in Happel and Brenner[26]) calculated the enhanced drag for small to moderate particle sizes (valid up to about $\lambda = 0.5$). The centerline lag coefficient is obtained readily from Faxen's law.[26] In terms of H and W, the results are[2]

$$H(\lambda) = \Phi[1 - 1.004\lambda + 0.418\lambda^2 + 0.21\lambda^4 - 0.169\lambda^5 + O(\lambda^6)] \qquad (19)$$

$$W(\lambda) = \frac{\Phi}{2}(3 - \Phi^2)\left[1 - \frac{\lambda^2}{3} + O(\lambda^3)\right] \quad (20)$$

where Φ is given by eq 12. Pozrikidis[27] calculated $K(\lambda, 0)$ and $G(\lambda, 0)$ for all particle sizes using a boundary integral method, but only graphical results were presented, making it difficult to update eqs 19 and 20.

B. Cross-Sectional Averaging for Diffusion. Ganatos et al.[28] calculated $K(\lambda, \beta)$ using a collocation method, and Weinbaum[24] averaged those results over the cross-section to obtain $H(\lambda)$ for $\lambda = 0.1$, 0.2, 0.333, 0.5, 0.667, and 0.8. The results for H were given in tabular form. By asymptotic matching of drag expressions for spheres near plane walls, Pawar and Anderson[29] found that, for $\lambda \rightarrow 0$,

$$H(\lambda) = 1 + \frac{9}{16}\lambda \ln \lambda - 1.19358\lambda + 0.159317\lambda^3 + O(\lambda^4) \quad (21)$$

which agrees very well with the results of Weinbaum[24] up to $\lambda = 0.33$. A least-squares fit to the results of Weinbaum[24] and Pawar and Anderson[29] gives

$$H(\lambda) = 1 + \frac{9}{16}\lambda \ln \lambda - 1.19358\lambda + 0.4285\lambda^3 - 0.3192\lambda^4 + 0.08428\lambda^5 \quad (22)$$

where the coefficient of λ^3 has been modified from that in eq 21 to improve the overall fit. Equation 22 gives results that are within 0.5% of those reported by Weinbaum.[24] Although fitted mainly to results for $\lambda \leq 0.8$, this expression also gives the correct limit of $H(1) = 0$.

The various results for H in slit pores are compared in Figure 5. Included are the centerline results (eq 20), the asymptotic results for small λ (eq 21), the cross-sectional average results of Weinbaum[24] (which we view as exact), and the curve fit (eq 22). It is seen that eq 22 accurately represents the cross-sectional averages. Unlike the situation for cylindrical pores, the centerline approximation in slit pores consistently overestimates H, with an rms error of 25%.

Another approach that has been used to predict diffusional hindrances in slits is to assume that the increased drag on a particle between parallel plates is the sum of two single-wall contributions, an approximation attributed to Oseen.[30] Using this linear superposition, together with the leading term in the single-wall results of Faxen (summarized in Happel and Brenner[26]), we obtained

$$K_d(\lambda) = 1 - \frac{\lambda}{(1-\lambda)f(\lambda)}\left[\frac{9}{8} - \frac{81\lambda}{128}\right]\tanh^{-1}\left[\frac{1-\lambda}{f(\lambda)}\right] \quad (23a)$$

$$f(\lambda) = \left[1 - \frac{81\lambda^2}{256}\right]^{1/2} \quad (23b)$$

This expression will be compared later with K_d predictions based on eqs 19 and 22 and with relative diffusivities measured by tracking particle motion in slits. Although quite accurate up to about $\lambda = 0.5$, it will be seen that eq 23 overestimates K_d for larger particles.

C. Cross-Sectional Averaging for Convection. For convection in slits, Staben et al.[31] obtained an asymptotic expression for K_c for $\lambda \rightarrow 0$. In terms of W, that result is

$$W(\lambda) = 1 - 3.02\lambda^2 + 2.02\lambda^3 + o(\lambda^3) \quad (24)$$

Those authors also used a boundary integral method to calculate

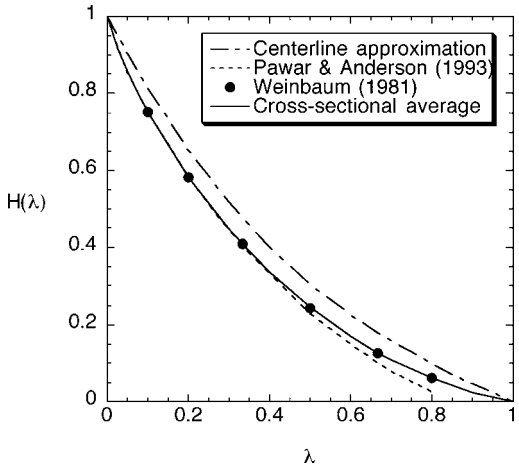

Figure 5. Diffusional hindrance factor (H) for a sphere in a slit pore, as a function of relative particle size (λ). Results based on centerline hydrodynamics (eq 19) are compared with those obtained by cross-sectional averaging. The latter include an asymptotic expression from Pawar and Anderson[29] for $\lambda \rightarrow 0$ (eq 21), numerical results from Weinbaum,[24] and a curve fit to the numerical, cross-sectional averages (eq 22).

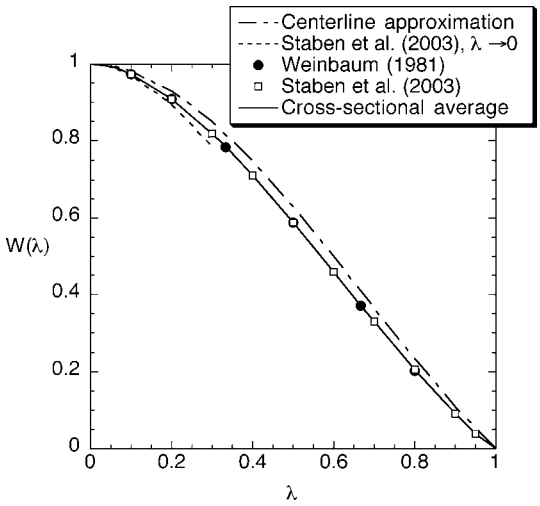

Figure 6. Convective hindrance factor (W) for a sphere in a slit pore, as a function of relative particle size (λ). Results based on centerline hydrodynamics (eq 20) are compared with those obtained by cross-sectional averaging. The latter include an asymptotic expression from Staben et al.[31] for $\lambda \rightarrow 0$ (eq 24), numerical results from Weinbaum[24] and from G of Staben et al.,[31] and a curve fit to the numerical, cross-sectional averages (eq 25).

$G(\lambda, \beta)$ for $\lambda = 0.1$, 0.2, ..., 0.9, and 0.95. Numerically integrating over β to obtain W at each λ, and using a least-squares fit to represent the results for all λ, we obtained

$$W(\lambda) = 1 - 3.02\lambda^2 + 5.776\lambda^3 - 12.3675\lambda^4 + 18.9775\lambda^5 - 15.2185\lambda^6 + 4.8525\lambda^7 \quad (25)$$

which is within 0.4% of the "exact" W for all sizes ($0 \leq \lambda \leq 0.95$). The coefficient of λ^3 in eq 25 was modified from that in eq 24 to improve the overall fit. Numerical results for W in slits are available also from Weinbaum,[24] for a smaller range of sizes ($0 \leq \lambda \leq 0.8$). The results of Weinbaum[24] agree with those derived from Staben et al.[31] to within 1%.

The various results for W in slits are compared in Figure 6, where it is seen that eq 25 represents either set of cross-sectional averages[24,31] very well. As expected, the asymptotic expression given by eq 24 is accurate up to about $\lambda = 0.1$. The centerline approximation given by eq 20 consistently overestimates W, with an rms error of 10%.

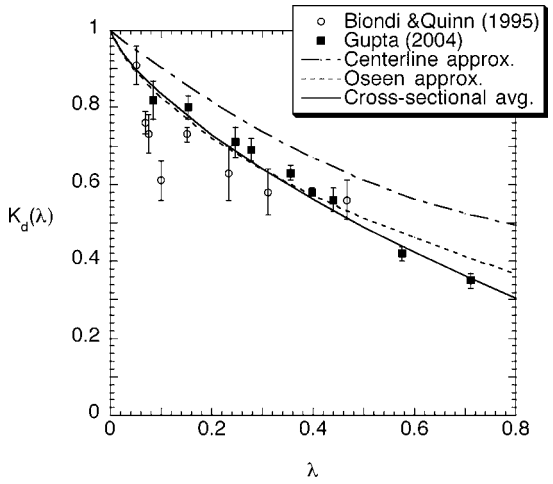

Figure 7. Particle diffusivity in a slit relative to that in bulk solution (K_d), as a function of relative particle size (λ). Experimental results of Biondi and Quinn[32] and Gupta[33] from particle tracking in microchannels are compared with predictions using centerline hydrodynamics (eq 19), the Oseen approximation (eq 23), or more rigorous cross-sectional averaging (eq 22).

Dividing eq 25 by $(1 - \lambda)$ yields K_c for a slit, which approaches unity for $\lambda \rightarrow 0$ and increases to a maximum of approximately 1.19 at $\lambda \cong 0.4$. In contrast to a cylindrical pore, in a slit $K_c \rightarrow 0$ as $\lambda \rightarrow 1$. In this limit the centerline approximation becomes exact and $G(\lambda, 0) = F^p/F^t$, where F^p is the force on a stationary sphere due to a Poiseuille flow (relative to the Stokes law force evaluated at the centerline velocity) and F^t is the force on a sphere translating in a quiescent fluid (again relative to Stokes law). As shown in Staben et al.,[31] F^p remains bounded as $\lambda \rightarrow 1$, whereas F^t from a lubrication analysis depends logarithmically on the gap between the sphere and the wall, ultimately varying as $\ln(1 - \lambda)$. Accordingly, $G \rightarrow 0$ and $K_c \rightarrow 0$ as $\lambda \rightarrow 1$. In other words, a tightly fitting sphere is not convected because the force due to the Poiseuille flow is unable to overcome the strong lubrication force that resists sphere motion.[27] This should be true not just for slits, but for any pore cross-section (e.g., square or rhomboid) that is not completely occluded by the largest sphere that will fit. Cylindrical channels are unique in that the fluid cannot bypass a sphere when $\lambda = 1$. Consequently, F^p and F^t are both unbounded as $\lambda \rightarrow 1$, the force balance in that limit yielding $G \rightarrow {}^1/_2$ and $K_c \rightarrow 1$.

Experimental Results

Recent studies involving microscopic visualization of the motion of individual particles in slits provide new tests of the hindrance factor predictions, supplementing earlier data from track−etch membranes.[2] Particle tracking experiments yield K_d or K_c, and in some cases even the local K or G, whereas transmembrane fluxes are influenced by partitioning and reflect H and/or W. Biondi and Quinn[32] observed diffusion of polystyrene beads of 2−9 μm diameter in 20−707 μm wide slits. Gupta[33] studied diffusion of carboxylated polystyrene beads of 0.11−0.93 μm diameter in 1.3−2.7 μm channels. In both cases the particles were free to sample various cross-sectional positions, so that what was measured was K_d. Figure 7 compares those two sets of data with some of the theoretical predictions. In general, the data are in good agreement with the cross-sectional average K_d (obtained by dividing H from eq 22 by $1 - \lambda$), especially those of the more recent experiments. All of the data fall below the centerline prediction (from eq 19). Also plotted is the Oseen approximation (eq 23), which agrees well with the more rigorous cross-sectional average up to about $\lambda = 0.5$, but overestimates K_d thereafter. Not shown are results from a similar experimental study by Fauncheux and Libchaber,[34] which exhibited much more scatter than the data in Figure 7.

The advent of optical tweezers has made it possible to obtain local measurements of the relative diffusivity (K^{-1}). Lin et al.[35] used optical tweezers and video microscopy to measure K^{-1} for 0.93 μm diameter poly(methyl methacrylate) spheres positioned near the mid-plane of glass slits with widths of 2−70 μm. Within experimental error, their results agree with predictions from centerline hydrodynamics. Dufresne et al.[30] used optical tweezers to observe diffusivities of polystyrene sulfate spheres of 1.1 μm diameter in an 8 μm slit, as a function of particle position (β). Again, the local values of K^{-1} so obtained were in good agreement with hydrodynamic predictions.

Concerning convection, Staben and Davis[36] tracked polystyrene particles with diameters of 36−495 μm in a 520 μm slit during pressure-driven flow. Particle positions were sufficiently restricted during their observations that they were able to obtain local values of G. As shown in their Figure 2, the data for $0.07 \leq \lambda \leq 0.95$ agreed with the theoretical lag coefficients of Staben et al.[31] to within experimental error. Accordingly, those results support the validity of eq 25, which was derived from the same set of predicted lag coefficients.

Conclusion

The hydrodynamic theory of hindered transport for neutral spheres in cylindrical or slit pores, pioneered more than 50 years ago, has finally reached a practical state of completion. Accurate expressions are available now for diffusive and convective hindrance factors in both geometries, properly averaged over the pore or channel cross-section. For calculations involving a wide range of relative particle sizes, we recommend eq 16 (diffusion in cylindrical pores), eq 18 (convection in cylindrical pores), eq 22 (diffusion in slits), and eq 25 (convection in slits). The predictions of the hydrodynamic theory are in good agreement with recent data from particle tracking experiments, as well as being supported by earlier studies using track−etch membranes.

Acknowledgment

P.D. is supported by a scholarship from the Ministry of Science, Technology and Environment of Thailand.

Literature Cited

(1) Einstein, A. On the Theory of the Brownian Movement. In *Investigations on the Theory of the Brownian Movement*; Furth, R., Ed.; Dover: New York, 1956; pp 19−35.

(2) Deen, W. M. Hindered Transport of Large Molecules in Liquid-Filled Pores. *AIChE J.* **1987**, *33*, 1409.

(3) Mitragotri, S. Modeling Skin Permeability to Hydrophilic and Hydrophobic Solutes Based on Four Permeation Pathways. *J. Controlled Release* **2003**, *86*, 69.

(4) Odde, D. Diffusion Inside Microtubules. *Eur. Biophys. J.* **1998**, *27*, 514.

(5) Burns, D. B.; Zydney, A. L. Contributions to Electrostatic Interactions on Protein Transport in Membrane Systems. *AIChE J.* **2001**, 47, 1101.

(6) Blom, M. T.; Chmela, E.; Oosterbroek, R. E.; Tijssen, R.; van den Berg, A. On-Chip Hydrodynamic Chromatography Separation and Detection of Nanoparticles and Biomolecules. *Anal. Chem.* **2003**, *75*, 6761.

(7) Brenner, H.; Gaydos, L. J. The Constrained Brownian Movement of Spherical Particles in Cylindrical Pores of Comparable Radius. *J. Colloid Interface Sci.* **1977**, *58*, 312.

(8) Bungay, P. M.; Brenner, H. The Motion of a Closely Fitting Sphere in a Fluid-Filled Tube. *Int. J. Multiphase Flow* **1973**, *1*, 25.

(9) Giddings, J. C.; Kucera, E.; Russell, C. P.; Myers, M. N. Statistical Theory for the Equilibrium Distribution of Rigid Molecules in Inert Porous Networks. Exclusion Chromatography. *J. Phys. Chem*. **1968**, *72*, 4397.

(10) Pappenheimer, J. R.; Renkin, E. M.; Borrero, L. M. Filtration, Diffusion and Molecular Sieving through Peripheral Capillary Membranes. *Am. J. Physiol*. **1951**, *167*, 13.

(11) Lane, J. A. Section II. In *Chemical Engineer's Handbook*; Perry, J. H., Ed.; McGraw-Hill: New York, 1950; p 753.

(12) Renkin, E. M. Filtration, Diffusion, and Molecular Sieving through Porous Cellulose Membrane. *J. Gen. Physiol*. **1954**, *38*, 225.

(13) Haberman, W. L.; Sayre, R. M. Motion of Rigid and Fluid Spheres in Stationary and Moving Liquids Inside Cylindrical Tubes. David W. Taylor Basin Report No. 1143; U.S. Navy: Washington, DC, 1958.

(14) Wang, H.; Skalak, R. Viscous Flow in a Cylindrical Tube Containing a Line of Spherical Particles. *J. Fluid Mech*. **1969**, *38*, 75.

(15) Paine, P. L.; Scherr, P. Drag Coefficients for the Movement of Rigid Spheres through Liquid-Filled Cylindrical Pores. *Biophys. J*. **1975**, *15*, 1087.

(16) Bean, C. P. The Physics of Porous Membranes--Neutral Pores. In *Membranes*; Eisenman, G., Ed.; Marcel Dekker: New York, 1972; Vol. 1, pp 1−54.

(17) Bowen, W. R.; Sharif, A. O. Transport through Microfiltration Membranes-Particle Hydrodynamics and Flux Reduction. *J. Colloid Interface Sci*. **1994**, *168*, 414.

(18) Bowen, W. R.; Mohammad, A. W.; Hilal, N. Characterisation of Nanofiltration Membranes for Predictive Purposes − Use of Salts, Uncharged Solutes and Atomic Force Microscopy. *J. Membr. Sci*. **1997**, *126*, 91.

(19) Feng, Z.; Michaelides, E. E. Hydrodynamic Force on Spheres in Cylindrical and Prismatic Enclosures. *Int. J. Multiphase Flow* **2002**, *28*, 479.

(20) Ben Richou, A.; Ambari, A.; Naciri, J. K. Correction Factor of the Stokes Force Undergone by a Sphere in the Axis of a Cylinder in Uniform and Poiseuille Flows. *Eur. Phys. J. Appl. Phys*. **2003**, *24*, 153.

(21) Nitsche, J. M.; Balgi, G. Hindered Brownian Diffusion of Spherical Solutes within Circular Cylindrical Pores. *Ind. Eng. Chem. Res*. **1994**, *33*, 2242.

(22) Mavrovouniotis, G. M.; Brenner, H. Hindered Sedimentation, Diffusion and Dispersion Coefficients for Brownian Spheres in Circular Cylindrical Pores. *J. Colloid Interface Sci.* **1988**, *124*, 269.

(23) Higdon, J. J. L.; Muldowney, G. P. Resistance Functions for Spherical Particles, Droplets and Bubbles in Cylindrical Tubes. *J. Fluid Mech*. **1995**, *298*, 193.

(24) Weinbaum, S. Strong Interaction Theory for Particle Motion through Pores and Near Boundaries in Biological Flows at Low Reynolds Number. *Lect. Math. Life Sci*. **1981**, *14*, 119.

(25) Ennis, J.; Zhang, H.; Stevens, G.; Perera, J.; Scales, P.; Carnie, S. Mobility of Protein through a Porous Membrane. *J. Membr. Sci.* **1996**, *119*, 47.

(26) Happel, J.; Brenner, H. *Low Reynolds Number Hydrodynamics*; Martinus Nijhoff: The Hague, The Netherlands, 1983; pp 67, 327.

(27) Pozrikidis, C. The Motion of Particles in the Hele-Shaw Cell. *J. Fluid Mech*. **1994**, *261*, 199.

(28) Ganatos, P.; Pfeffer, R.; Weinbaum, S. A Strong Interaction Theory for the Creeping Motion of a Sphere between Plane Parallel Boundaries Part 2. Parallel Motion. *J. Fluid Mech*. **1980**, *99*, 755.

(29) Pawar, Y.; Anderson, J. L. Hindered Diffusion in Slit Pores: An Analytical Result. *Ind. Eng. Chem. Res*. **1993**, *32*, 743.

(30) Dufresne, E. R.; Altman, D.; Grier, D. G. Brownian Dynamics of a Sphere Between Parallel Walls. *Europhys. Lett*. **2001**, *53*, 264.

(31) Staben, M. E.; Zinchenko, A. Z.; Davis, R. H. Motion of a Particle between Two Parallel Plane Walls in Low-Reynolds-Number Poiseuille Flow. *Phys. Fluids* **2003**, *15*, 1711. (For errata see *Phys. Fluids* **2004**, *16*, 4206).

(32) Biondi, S. A.; Quinn, J. A. Direct Observation of Hindered Brownian Motion. *AIChE J*. **1995**, *41*, 1324.

(33) Gupta, M. Polymer and Sphere Diffusion in Confinement. M.S. Thesis, Massachusetts Institute of Technology, Cambridge, MA, 2004.

(34) Faucheux, L. P.; Libchaber, A. J. Confined Brownian Motion. *Phys. Rev. E*: *Stat. Phys., Plasmas, Fluid, Relat. Interdiscip. Top*. **1994**, *49*, 5158.

(35) Lin, B.; Yu, J.; Rice, S. A. Direct Measurement of Constrained Brownian Motion of an Isolated Sphere between Two Walls. *Phys. Rev. E: Stat. Phys., Plasmas, Fluid, Relat. Interdiscip. Top.* **2000**, *62*, 3909.

(36) Staben, M. E.; Davis, R. H. Particle Transport in Poiseuille Flow in Narrow Channels. *Int. J. Multiphase Flow* **2005**, *31*, 529.

Received for review December 13, 2005
Revised manuscript received February 2, 2006
Accepted February 3, 2006

IE051387N